Breakup reactions of the halo nuclei ^{11}Be and ^{8}B

Kai Hencken and George Bertsch
Institute for Nuclear Theory, University of Washington, Seattle, Washington 98195

Henning Esbensen
Physics Division, Argonne National Laboratory, Argonne, Illinois 60439

(Received 25 July 1996)

We calculate the nuclear induced breakup of ^{11}Be and ^{8}B using a more realistic treatment of the diffraction and stripping processes than in previous work. The breakup is treated in the eikonal approximation with a profile function calculated from a realistic optical potential at low energies and from free nucleon-nucleon cross sections at high energies. This treatment gives a good description of measured breakup cross sections, as well as the longitudinal momentum distribution of the corelike fragments, which is narrower than predicted in the transparent limit. The real part of the potential is found to be significant and enhances the diffractive breakup at low energies. [S0556-2813(96)01712-8]

PACS number(s): 25.60.Gc, 24.10.−i, 25.70.Mn

I. INTRODUCTION

Breakup reactions of light nuclei near the neutron or proton drip line have demonstrated the existence of nuclei with a halo composed of one or two loosely bound nucleons. The momentum distribution of the fragments becomes much narrower in halo nuclei, and it is common to interpret these distributions in terms of the momentum-space wave function of the halo nucleus. This picture is overly simplified and more microscopic modeling of the reaction process is needed to interpret the distributions [1,2].

In this work we investigate this question further using realistic projectile-target interactions. We calculate the breakup of ^{11}Be and ^{8}B by a nuclear target using the eikonal approximation for the reaction theory. This is essentially the model developed by Serber [3] and Glauber [4] to describe the breakup of the deuteron, improved beyond the black-disk approximation used in that original work [5]. Our interaction will be taken from a realistic optical potential at low energies and from total nucleon-nucleon cross sections at high energies.

There are two different processes by which the breakup occurs, namely stripping and diffraction. We present the theory of these processes in the next section. Stripping depends only on the absorption interaction, while diffraction is quite sensible to the real part as well. Our interaction includes both, as described in Sec. III. Details of the numerical calculations are described in Sec. IV. Results for the total cross section are discussed in Sec. V, the longitudinal momentum distributions in Secs. VI and VII.

Calculations using similar approaches have been done already in the past [6–9]. The idea of using the momentum distribution to investigate the wave function of the nucleus was first studied in [10]. Our aim is to have a model, with which one may calculate total cross sections and momentum distributions with a realistic reaction model. A calculation of the momentum distribution alone was done recently [11] using a much more schematic treatment of the reaction model. Our results are similar to their findings, justifying to some extent their simplifications.

II. PROBABILITIES AND CROSS SECTIONS IN THE DIFFRACTIVE MODEL

We consider a single-particle model of the halo nucleus. The ground state is described by a wave function $\phi_0(\vec{r})$ which depends on the relative coordinate $\vec{r}$ between the nucleon and the core.

After interacting with a target, the wave function of the halo nucleus in its rest frame has the form

$$\Psi(\vec{r},\vec{R}) = S_n(\vec{b}_n) S_c(\vec{b}_c)\, \phi_0(\vec{r}), \tag{1}$$

where $\vec{R}$ is the coordinate of the center of mass of the halo nucleus, and $\vec{b}_c$ and $\vec{b}_n$ are the impact parameters of the core and the nucleon with respect to the target nucleus, i.e., $\vec{b}_n = \vec{R}_\perp + \vec{r}_\perp A_c/(A_c+1)$ and $\vec{b}_c = \vec{R}_\perp - \vec{r}_\perp/(A_c+1)$, where A_c is the mass number of the core. The two profile functions, $S_n(\vec{b}_n)$ for the nucleon and $S_c(\vec{b}_c)$ for the core, are generated by interactions with the target nucleus. In the eikonal approximation, they are defined by the longitudinal integrals over the corresponding potentials:

$$S(\vec{b}) = \exp\left[\frac{-i}{\hbar v}\int dz\, V(\vec{b}+z\hat{z})\right], \tag{2}$$

where v is the beam velocity. The potential V is the full optical potential, including the Coulomb potential and the real and imaginary parts of the nuclear potential. The scattering wave function is the difference between Eq. (1) and the wave function of the undisturbed beam,

$$\Psi_{\rm scat} = (S_n S_c - 1)\,\phi_0. \tag{3}$$

Elastic and diffractive scattering are calculated by taking overlaps of $\Psi_{\rm scat}$ with different final states. For elastic scattering, we take the overlap with the halo nucleus in its ground state, but with some arbitrary transverse momentum $\vec{K}_\perp$. This is

$$a(\vec{K}_\perp) = \int d^2\vec{R}_\perp e^{-i\vec{K}_\perp\cdot\vec{R}} \int d^3\vec{r}\,\phi_0^*(\vec{r})(S_c S_n - 1)\,\phi_0(\vec{r}). \tag{4}$$

The differential and total elastic cross sections are then given by

$$\frac{d\sigma_{\rm el}}{d^2\vec{K}_\perp} = \frac{|a(\vec{K}_\perp)|^2}{(2\pi)^2}, \tag{5}$$

$$\sigma_{\rm el} = \int d^2\vec{R}_\perp \left| \int d^3\vec{r}\,\phi_0^*(\vec{r})(S_c S_n - 1)\,\phi_0(\vec{r}) \right|^2. \tag{6}$$

In the case of ^{8}B, where the proton is in a p state, we have to sum also over the final and average over the initial M states:

$$\sigma_{\rm el} = \frac{1}{2L_0+1} \sum_{M_0, M_0'} \int d^2\vec{R}_\perp \left| \int d^3\vec{r}\,\phi_{0,M_0'}^*(\vec{r})(S_c S_n - 1)\,\phi_{0,M_0}(\vec{r}) \right|^2. \tag{7}$$

For diffractive breakup the final state depends on the relative momentum $\vec{k}$ of nucleon and core in their center-of-mass frame as well as on the transverse momentum $\vec{K}_\perp$ of the center of mass. Writing the continuum nucleon-core wave function as $\phi_{\vec{k}}(\vec{r})$, the diffractive breakup cross section is given by

$$\frac{d\sigma_{\rm diff}}{(d^2\vec{K}_\perp d^3\vec{k})} = \frac{1}{(2\pi)^5} \frac{1}{2L_0+1} \sum_{M_0} \left| \int d^3\vec{r} d^2\vec{R}_\perp e^{-i\vec{K}_\perp\cdot\vec{R}_\perp} \phi_{\vec{k}}^*(\vec{r}) S_c S_n \phi_{0,M_0}(\vec{r}) \right|^2. \tag{8}$$

Here the continuum wave function is normalized asymptotically to a plane wave, $\phi_{\vec{k}} \sim \exp(i\vec{k}\cdot\vec{r})$. If we are only interested in the relative momentum distribution, i.e., in $\vec{k}$, we can integrate over $\vec{K}_\perp$ to get

$$\frac{d\sigma_{\rm diff}}{d^3\vec{k}} = \frac{1}{(2\pi)^3} \frac{1}{2L_0+1} \sum_{M_0} \int d^2\vec{R}_\perp \left| \int d^3\vec{r}\,\phi_{\vec{k}}^*(\vec{r}) S_c S_n \phi_{0,M_0}(\vec{r}) \right|^2. \tag{9}$$

A convenient expression for the total diffractive cross section can be derived if ϕ_0 is the only bound state of the system. This is

$$\sigma_{\rm diff} = \frac{1}{2L_0+1} \sum_{M_0} \int d^2\vec{R}_\perp \left[\int d^3\vec{r}\,\phi_{0,M_0}(\vec{r})^* |S_c S_n|^2 \phi_{0,M_0}(\vec{r}) - \sum_{M_0'} \left| \int d^3\vec{r}\,\phi_{0,M_0'}(\vec{r})^* S_c S_n \phi_{0,M_0}(\vec{r}) \right|^2 \right]. \tag{10}$$

Other contributions to the total cross section come from absorption, present when the eikonal factors have moduli less than 1. There are three of these so-called stripping processes. The nucleon-absorption cross section, differential in the momentum of the core, is given by

$$\frac{d\sigma_{n\ \rm str}}{d^3\vec{k}_c} = \frac{1}{(2\pi)^3} \frac{1}{2L_0+1} \sum_{M_0} \int d^2\vec{b}_n [1 - |S_n(\vec{b}_n)|^2] \left| \int d^3\vec{r} e^{-i\vec{k}_c\cdot\vec{r}} S_c(\vec{b}_c)\,\phi_{0,M_0}(\vec{r}) \right|^2. \tag{11}$$

The corresponding total cross section for stripping of the nucleon is

$$\sigma_{n\ \rm str} = \frac{1}{2L_0+1} \sum_{M_0} \int d^2\vec{b}_n [1 - |S_n(\vec{b}_n)|^2] \int d^3\vec{r}\,\phi_{0,M_0}(\vec{r})^* |S_c(\vec{b}_c)|^2 \phi_{0,M_0}(\vec{r}). \tag{12}$$

The stripping of the core is expressed in a similar way, interchanging subscripts n and c.

Finally, the expression for absorption of both nucleon and core is given by

$$\sigma_{\rm abs} = \frac{1}{2L_0+1} \sum_{M_0} \int d^2\vec{b}_c [1 - |S_c(\vec{b}_c)|^2] \int d^3\vec{r}\,\phi_{0,M_0}(\vec{r})^* [1 - |S_n(\vec{b}_n)|^2] \phi_{0,M_0}(\vec{r}). \tag{13}$$

All of the above contributions have been written in the form of an integration over some transverse coordinate, so the integrand may be interpreted as an impact-parameter-dependent probability. Note, however, that for the diffraction and the elastic scattering, the integration is over the impact parameter with respect to the center of mass, whereas it is over the impact parameter with respect to the nucleon or the core for the stripping and absorption processes. For the total cross sections we can change the integration variable to the center-of-mass impact parameter in these cases. All the different probabilities together with the one for no interaction then add up to one, showing that all possible processes are included in this scheme.

Note also that the diffractive differential cross section [Eq. (9)] is expressed as a function of the relative momentum, i.e., the momentum of the nucleon or the core in the nucleon-core center-of-mass frame. No expression of the same form exists for the nucleon or core momenta due to the interplay with the diffraction of the center-of-mass motion.

III. THE POTENTIAL FOR THE NUCLEON-TARGET AND CORE-TARGET INTERACTION

Evaluation of the profile functions requires a potential model for the interaction between the target nucleus and the constituents of the halo nucleus. At low energies, extending up to about 100 MeV/nucleon, one can find optical potentials that are fit to nucleon-nucleus scattering. We use the potential of [12], which was fit to scattering data in the range 10–60 MeV. The potential has the usual Woods-Saxon form, with volume and surface imaginary terms. We drop the spin-orbit term, which has a small effect on spin-independent observables. This potential can be used as it stands for the target-nucleon interaction. We apply it to the core-target interaction by folding it with the core density distribution,

$$V_c(r)=\int d^3\vec{x}\rho_c(x)V_{\rm op}(|\vec{r}-\vec{x}|). \tag{14}$$

For the core density we use a harmonic oscillator density with parameters taken from the charge distribution of the core nucleus [13] ($a=1.79$ fm and $\alpha=0.61$ fm for the ^{10}Be and similar for ^{7}Be).

At high energies, many-body effects on the effective interaction are small, and we may use the free nucleon-nucleon interaction to generate the potentials. Following [14–16], we ignore the finite range of the NN interaction and take the potential to be proportional to the density of the target

$$V_\rho(r)=V_0\rho_t(r). \tag{15}$$

We have either a harmonic oscillator or a Fermi form for the target density distribution and use the tabulated width and diffuseness [13]. We assume that protons and neutrons have the same density distribution.

The imaginary part of V_0 can be determined from free NN cross sections. The result for the neutron-target interaction is

$$\mathrm{Im}[V_n(r)]=-\frac{1}{2}\hbar v(Z_T\sigma_{np}+N_T\sigma_{nn})\rho_t(r), \tag{16}$$

where the spatial integral of the target density is normalized to one, and a similar formula for the proton-target interaction. Here Z_T and N_T are the proton and neutron numbers, respectively, of the target nucleus, and the σ's are the total NN cross sections. The core-nucleus interaction is generated by folding as it was done earlier for the optical potential. The total NN cross sections are calculated from the velocity-dependent parametrization given in [17].

The real part of the potential becomes small above 200 MeV and is negligible at 800 MeV [18]. We have neglected it in our calculations of the breakup at high energy. We shall also neglect the Coulomb part of the interaction, which makes a negligible contribution to breakup cross sections on light nuclei. Unfortunately, the Coulomb field may nevertheless affect the transverse momentum distributions. We therefore restrict our study to total cross sections and longitudinal momentum distributions.

IV. NUMERICAL CALCULATION OF THE PROBABILITIES

As seen in Sec. II, the cross sections all require calculating probability functions depending on the impact parameter, that have the form

$$\frac{d^3P_\Omega(b)}{d^3\vec{k}}=\frac{1}{(2\pi)^3}\left|\int d^3\vec{r}\;\;\phi_{\vec{k}}^*(\vec{r})\Omega(\vec{b},\vec{r}_\perp)\phi_0(\vec{r})\right|^2, \tag{17}$$

with an appropriate chosen Ω.

The wave functions ϕ_0 and $\phi_{\vec{k}}$ are determined as eigenfunction for a Woods-Saxon potential together with the Coulomb potential of a homogeneous charged sphere in the case of ^{8}B.

The ground state of ^{11}Be has spin parity of $1/2^+$, so we take an s wave,

$$\phi_0(r)=\frac{g(r)}{r}\;\;Y_{00}. \tag{18}$$

With our geometry of the Woods-Saxon potential ($R=2.7$ fm and $a=0.52$ fm [1]), the empirical neutron binding energy of 0.503 MeV is reproduced with a well depth of about $V_0=-61.1$ MeV.

For calculating diffractive cross sections, we expand the continuum wave function $\phi_{\vec{k}}$ in the usual partial wave representation,

$$\phi_{\vec{k}}(\vec{r})=\frac{4\pi}{k}\sum_{L,M}\;i^Le^{-i\delta_L}\frac{u_L(r)}{r}Y_{L,M}^*(\hat{k})Y_{L,M}(\hat{r}). \tag{19}$$

Here the δ_L are the phase shifts and $u_L(r)$ are the (real) solutions of the radial Hamilton operator. The probability is then given by

$$\frac{d^3P_\Omega(b)}{d^3\vec{k}}=\frac{1}{(2\pi)^3(2L_0+1)}\left(\frac{4\pi}{k}\right)^2\sum_{M_0}\left|\int d^3\vec{r}\sum_{L,M}(-i)^L e^{i\delta_L}Y_{L,M}(\hat{k})Y^*_{L,M}(\hat{r})\frac{u_L(r)}{r}\Omega(\vec{b},\vec{r}_\perp)\frac{g(r)}{r}Y_{L_0,M_0}(\hat{r})\right|^2. \quad (20)$$

As the direction of the impact parameter is not observed, we can integrate over the transverse angle of the momenta φ_k to get the double-differential probability

$$\frac{d^2P_\Omega(b)}{dk_l dk_\perp}=k_\perp\int d\varphi_k\frac{d^3P_\Omega(b)}{d^3\vec{k}} \quad (21)$$

$$=\frac{2\pi k_\perp}{(2\pi)^3(2L_0+1)}\left(\frac{4\pi}{k}\right)^2\sum_{M,M_0}\left|\int d^3\vec{r}\sum_{L}(-i)^L e^{i\delta_L}\widetilde{Y}_{L,M}(\theta_k)Y^*_{L,M}(\hat{r})\frac{u_L(r)}{r}\Omega(\vec{b},\vec{r}_\perp)\frac{g(r)}{r}Y_{L_0,M_0}(\hat{r})\right|^2. \quad (22)$$

In deriving this we have used the orthogonality of the spherical harmonics with respect to integration over φ_k and we define $\widetilde{Y}_{L,M}(\theta_k)\equiv Y_{L,M}(\hat{k})e^{-iM\varphi_k}$, i.e., the spherical harmonic without the φ_k-dependent part.

The numerical integration will be performed in spherical coordinates as follows:

$$\frac{d^2P_\Omega(b)}{dk_l dk_\perp}=2\pi k_\perp\frac{1}{(2\pi)^3(2L_0+1)}\left(\frac{4\pi}{k}\right)^2\sum_{M,M_0}\left|\int dr\int d\cos\theta\left[\sum_L(-i)^L e^{i\delta_L}\widetilde{Y}_{L,M}(\theta_k)u_L(r)g(r)\widetilde{Y}_{L,M}(\theta)\widetilde{Y}_{L_0,M_0}(\theta)\right]\right.$$
$$\left.\times\int d\varphi\exp[i(M_0-M)\varphi]\Omega(\vec{b},\vec{r}_\perp)\right|^2. \quad (23)$$

As Ω is an even function in φ, we can replace $\exp(i\varphi)$ by $\cos(\varphi)$ in the last expression. Note that the summation over L and the integration over φ are independent of each other, and therefore the integration over φ has to be done only one time instead of L times for the sum. There are several advantages to using this expression from a numerical point of view. The number of φ integrations is lower by a factor of L due to the factorization. Only one integration over the coordinates has to be done, which then has to be squared. And finally, by doing the θ integration inside the r integration, we can minimize the number of wave-function evaluations, which is normally a rather calculation-intensive step. Angular momenta up to $l=5$ or $l=7$ have been used throughout the calculation. The cross section for the different processes can then be found by integrating over the impact parameter. Longitudinal momentum distributions are found by integrating also over the transverse momenta. For these three integrations we have used a Gaussian integration with a fixed number of points.

For better numerical convergence in the calculation of diffractive excitation, we replace the operator $\Omega=S_cS_n$, by $\Omega=S_cS_n-1$, which are of course equivalent for transition matrix elements.

In order to test the accuracy of our calculation we have compared the results of the differential cross sections integrated over all k and the separate calculation of the total cross section directly from Eq. (10). Both results were found to agree within a few percent. Therefore our results should be accurate to a few percent.

For the calculation of the stripping probabilities, we use the same Eq. (17), replacing the scattering wave by a plane wave. Thus the phase shifts are set to zero and the continuum partial waves $u_L(r)$ are replaced by the spherical Bessel functions, $j_L(kr)$.

We do the same in the case of ^{8}B and use a p wave for the valence proton in the ground state. The parameters of the Wood-Saxon potential in this case are $R=2.48$ fm and $a=0.52$ fm. We include also the Coulomb potential of a homogeneous charged sphere with the same radius as the core in the calculation of bound and continuum states. The binding energy of 0.137 MeV is reproduced by a well depth of about $V_0=-47.5$ MeV.

V. INTEGRATED CROSS SECTIONS

We first show our calculated results for the integrated breakup cross sections for ^{11}Be. The diffractive and the three stripping cross sections are shown in Fig. 1 as functions of the target mass A. The largest component is core stripping, as might be expected. The absorption of both core and neutron is next. The sum of both vary with A roughly as the geometric size, i.e., as $(A_c^{1/3}+A^{1/3})^2$. The absorption cross section increases faster with A at high energies than at low energies, showing the deviation from a black disk. The diffractive component is quite small at 800 MeV/nucleon, but it has the same size as the neutron absorption at 40 MeV/nucleon. The difference is due to the real part of the potential, which is important at low energies and increases the diffractive scattering. At low energies diffraction and neutron stripping are of the same magnitude for all A. This agrees with other calculations [19,20] which find also that both processes are almost the same up to energies of 100 MeV/nucleon.

In Fig. 2 we compare our results with experiments. In one kind of experiment, the core fragment is detected in the reaction, so the processes that contribute are diffraction and neutron absorption. The solid lines show the theoretical cross sections to which we have added Coulomb excitation cross sections (dot-dashed line) obtained in [2] from the same

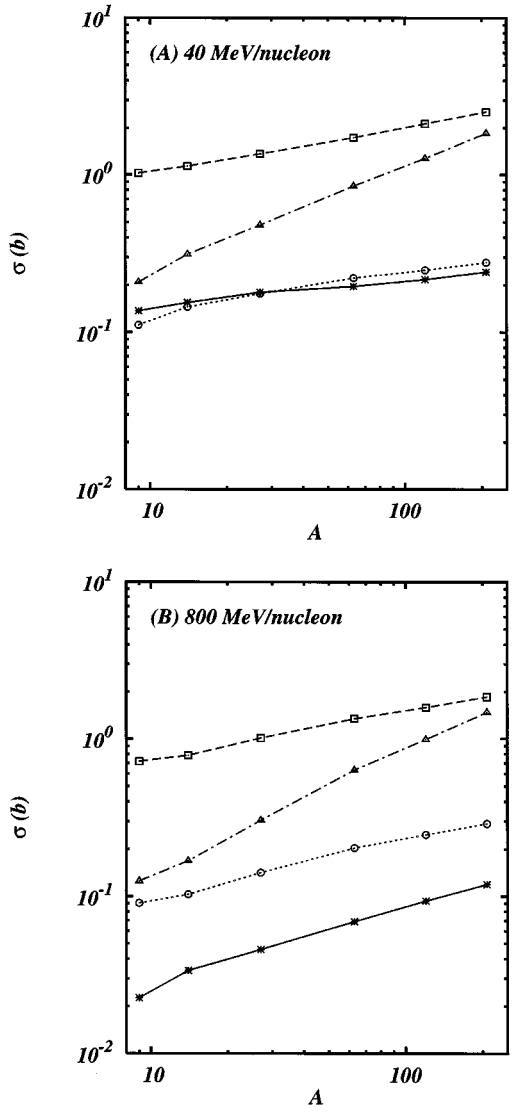

FIG. 1. Cross sections for the different nuclear induced breakup processes as functions of the target mass number A. Results are shown for a beam energy of 40 MeV/nucleon (a) and 800 MeV/nucleon (b). Shown are the cross sections for diffraction (solid line and stars), for the stripping of the neutron (dotted line and circles) and the core (dashed line and boxes) and for the absorption of both neutron and core (dash-dotted line and triangles).

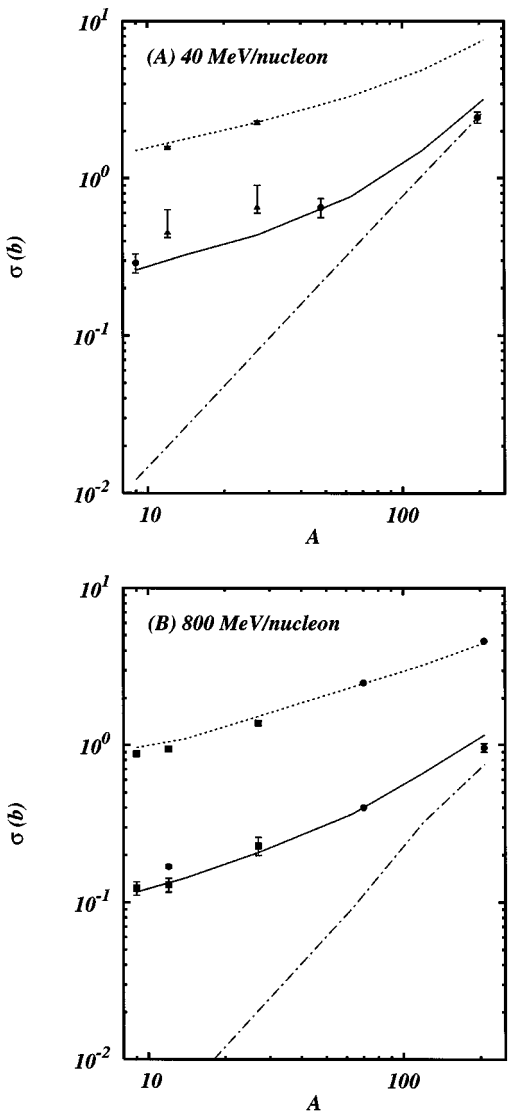

FIG. 2. Comparison of the neutron-removal cross section (solid line) and the total interaction cross section (dashed line) with experiments. We give the results again for an energy of 40 MeV/nucleon (a) and 800 MeV/nucleon (b). Also shown are the results for the Coulomb breakup, which were added to our results. The experimental results are from [21–25]. Please note that the results from [22] [triangles in (a)] are for an energy of 33 MeV/nucleon; the deviation from the calculated results is therefore partly due to this.

single-particle model. The theory agrees well with the data, taken from [21–25]. The two triangular data points in (A), which are somewhat high, are the results of [22] and are measured at an energy of 33 MeV/nucleon. The squares for the one-neutron removal at 800 MeV/nucleon are calculated by taking the difference of the interaction cross section between ^{11}Be and ^{10}B in [24]. The agreement at low energy is only possible because of the inclusion of the real part of the potential, which enhances the diffraction component. The dotted line shows the calculated total interaction cross sections. These are also in good agreement with experiment [21–25], as might be expected for a quantity that is determined mainly by the geometric size.

In Fig. 3 we show the dependence on the projectile energy. We have calculated the cross section using the optical potential between 20 and 200 MeV/nucleon and using free NN cross sections between 100 and 800 MeV/nucleon. All cross sections seem to have a smooth transition between the low energy and high energy model between 100 and 200 MeV.

The energy dependence clearly illustrates the deviation of the cross section from a black disk. The stronger dependence for a C target agrees with the expectation, as it is surface-dominated and therefore less a black disk than heavier targets (not shown). We also see a stronger dependence on the energy for those processes where a neutron is involved, again in agreement with our expectation. At high energies the total cross section follows more or less the energy dependence of the NN cross section. At low energies we have a rapid decrease of the diffraction cross section at 100 MeV/nucleon.

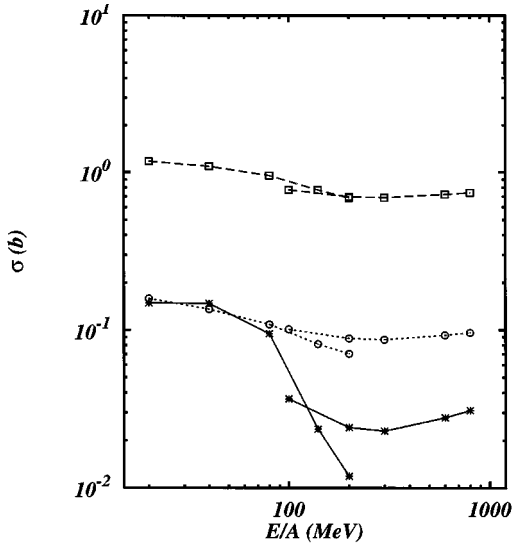

FIG. 3. The dependence of the total cross sections on the projectile energy E is shown for a C target. The notation is the same as in Fig. 1. The curves at lower energies are calculated with the optical potential, the curves at higher energies using the target density and free NN cross sections.

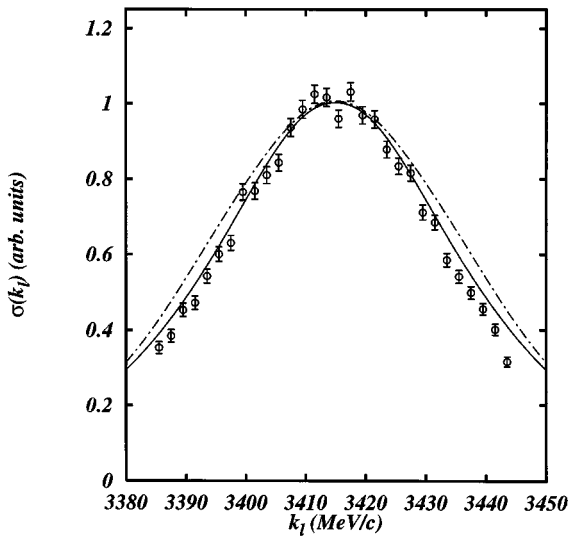

FIG. 4. Longitudinal momentum distribution of ^{10}Be fragments, produced in the breakup of ^{11}Be at 66 MeV/nucleon on a ^{9}Be target. The experimental results are from [26]. The solid line is the result of the full calculation for diffraction and stripping. The dotted line is the result of stripping in the transparent limit.

This is due to the decrease of the real part of the optical potential in this region. As already discussed in Fig. 1, the cross sections for diffraction and neutron stripping are almost the same at energies below 100 MeV/nucleon in agreement with other calculations [19,20].

VI. DIFFERENTIAL CROSS SECTIONS FOR ^{11}Be

We now discuss the differential cross sections for the momentum distributions in the final state. The neutron-stripping cross section has often been calculated in an approximation called the ''transparent limit.'' There one neglects the effect of the interaction between the observed fragment and the target nucleus and uses the expression

$$\frac{d\sigma_{\mathrm{n\ str,transp}}}{d^3\vec{k}_c}=\frac{1}{(2\pi)^3}\frac{1}{2L_0+1}\sum_{M_0}\int d^2\vec{b}_n[1-|S_n|^2]\times\left|\int d^3\vec{r}e^{-i\vec{k}_c\cdot\vec{r}}\phi_{0,M_0}(\vec{r})\right|^2, \tag{24}$$

which follows from Eq. (11) simply by setting $S_c=1$. With this approximation one gets a simple interpretation of the momentum distribution as the Fourier transform of the wave function of the ground state. The use of this approximation was questioned recently [1]. First of all, the total cross section is much too large. Moreover, the additional factor of S_c in Eq. (11) weights the amplitudes more heavily where the neutron is far from the core, and its momentum is lower. This leads to a narrower momentum distribution in the full theory. Another objection to the identification of final state momentum distributions with the Fourier transform of the projectile wave function is that the diffractive component does not behave this way at all, since the final state is not a plane wave.

In the comparison with experimental data, we consider only the longitudinal differential cross section. The longitudinal distributions are much easier to calculate and to interpret. The profile functions do not introduce any longitudinal momentum in the system, so one is rather insensible to the details of the potentials. When one looks at transverse distributions, there is not only a dependence on the shape of the profile functions, but higher-order scattering effects can also be significant. For the kinematic regime we are treating here, elastic scattering affects the transverse momentum much more strongly than the longitudinal momentum. Furthermore we get a simple equation for the diffraction only for the relative momentum. Relating this to the transverse momentum distribution of either of the fragments is not trivial, but requires a complete independent calculation, as different impact parameters interfere coherently in this case.

Let us now examine the longitudinal momentum distribution of the ^{10}Be fragment. Figure 4 shows the comparison of theory with a measurement on a ^{9}Be target at a beam energy of 66 MeV/nucleon [26]. The calculation of the solid curve includes both diffraction and neutron absorption. The two components are of similar size and shape. We also show the result of the transparent limit as the dot-dashed curve. We find, in agreement with [1], that the full calculation has a narrower momentum distribution than the transparent limit.

We have fitted the momentum distribution to a Lorentzian and also to a sum of two Gaussians. From the fit to a Lorentzian we get a FWHM Γ of 41.4 MeV/c for the full calculation and of 44.5 MeV/c for the transparent limit (always in the rest frame of ^{11}Be). The results of the full calculation are in good agreement with the experimental result of 41.6 ± 2.1. The individual contributions have a width of $\Gamma=41.2$ for diffraction and of 41.6 for stripping.

Fitting to a sum of two Gaussians we get a good description of our results. The width σ_0 of the narrow component is 22.2 MeV/c for the full calculation (19.6 MeV/c for diffraction and 25.2 for stripping) and 28.7 MeV/c for the transpar-

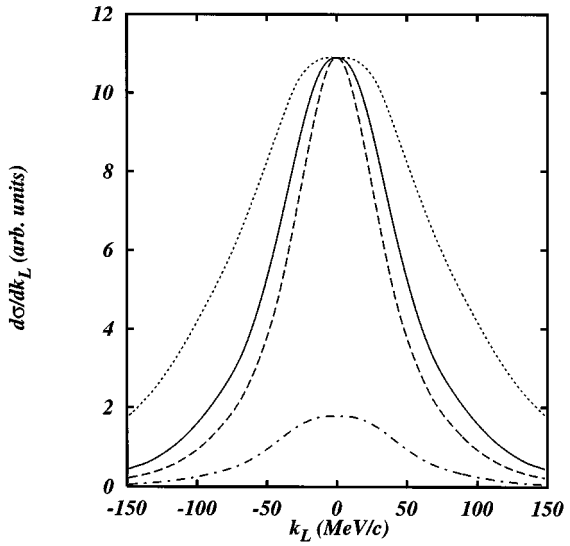

FIG. 5. Longitudinal momentum distribution of ^{7}Be fragments, produced in the breakup of ^{8}B at 1470 MeV/nucleon on a ^{12}C target. The solid line is the result of the full calculation for diffraction and stripping, the dash-dotted line the contribution to this from diffraction. The dashed line is the contribution of the $M\neq 0$ states to the total result. The dotted line is the result for stripping in the transparent limit.

ent limit. Our fit to the data gives $\sigma_0 = 22.1$ MeV/c, again in good agreement with the full calculation but not with the transparent limit.

VII. DIFFERENTIAL CROSS SECTIONS FOR ^{8}B

The breakup of ^{8}B was measured in [27] at 1471 MeV/nucleon for different targets and interpreted using the transparent limit of the Serber model. The observed width was found to be a factor of 2 smaller than the theory, showing that the transparent limit is a poor approximation in this case. The discrepancy is worse than for ^{11}Be because of the p-wave character of the halo nucleon. The $M=0$ state has the widest distribution in the longitudinal direction because of its longitudinal node, but it is suppressed in the full treatment because the proton and the core are aligned along the beam axis. We calculate the momentum distribution for a ^{12}C target as total cross section are given for this case. For the free NN cross section we use $\sigma_{nn}=47$ mb and $\sigma_{np}=44$ mb.

The results for our calculation with a realistic profile function are shown in Fig. 5. The dotted line shows the result for the transparent limit (only stripping), the solid line the result of the full calculation. We show two contributions to the full calculation: The dash-dotted line is the result for diffraction, which contributes to the order of 20%, the dashed line is the contribution of the $M\neq 0$ substates of the p wave. As one can see, the narrow width is mainly due to these states.

Fitting the curves with a Lorentzian, we get a FWHM Γ of 88 MeV/c for the full calculation (93 MeV/c for diffraction alone) and of 151 MeV/c for the transparent limit. Our results are in agreement with the experimental result of 81 ± 6 MeV/c.

We get the total interaction cross section $\sigma_I(^{8}\mathrm{B})$ as 838 mb and the proton-removal cross section $\sigma(^{8}\mathrm{B},^{7}\mathrm{Be})$ as 69 mb in fair agreement with the experimental results (809 ± 11 mb and 94 ± 4 mb, respectively). The discrepancy especially with the proton-removal cross section can only partly be attributed to our folding model, which is not a very good approximation for the core. A more detailed model [2], which uses the core wave functions, gets a larger cross section but is still smaller than the experimental result.

Comparing with the results at 790 MeV/nucleon and also for a ^{12}C target [24,28] we get a total interaction cross section of 796 mb, which compares well with the recent experimental value of 798 ± 6 mb. The proton-removal cross section can be calculated as the difference between the total cross sections of ^{8}B and ^{7}Be. We get $\sigma_I(^{8}\mathrm{B}) - \sigma_I(^{7}\mathrm{Be}) = 60\pm 11$ mb compared to our result of $\sigma(^{8}\mathrm{B},^{7}\mathrm{Be}) = 66$ mb.

The discrepancy between the 790 and 1471 MeV/nucleon data is disturbing. As the difference between the free NN cross sections in both cases is only of the order of 10%, one would expect to get similar results in both cases. The proton-removal cross section is only weakly sensible to the core interaction, but is more sensible to the parameters of the potential, especially its radius. Using, for example, a potential with $R=2.678$ fm at 1471 MeV/nucleon we get total cross section of $\sigma_I(^{8}\mathrm{B})=842$ mb and $\sigma(^{8}\mathrm{B},^{7}\mathrm{Be})=74$ mb. The proton removal cross section could therefore be used to calibrate the radius of the potential. But both measurements would give different results for this. It is therefore important to resolve this discrepancy, for example, by a direct measurement of σ_{1p} at 790 MeV/nucleon. The determination of the size of the core potential is crucial for the prediction of the S factor for the $p+^{7}\mathrm{Be}\rightarrow{}^{8}\mathrm{B}$ radiative capture process, see, e.g., [29].

VIII. SUMMARY AND CONCLUSIONS

The experimental results for the nuclear induced breakup of ^{11}Be on light targets, namely the total cross section and the longitudinal momentum distribution of ^{10}Be fragments, can be reproduced in the eikonal model using a single-particle description of the halo nucleon and using realistic potentials to generate the profile functions. The real part of the optical potential is clearly needed at lower beam energies (say below 100 MeV/nucleon) in order to reproduce the measured one-neutron removal cross sections. At higher energies the interaction deviates from the black-disk model due to the smallness of the nucleon-nucleon interaction.

In order to get a good agreement with measured longitudinal momentum distributions of ^{10}Be fragments, one needs to use the full expression for the differential cross section. Calculations based on the transparent limit of the stripping process, on the other hand, produce distributions that are too wide (resulting in a prediction of a wider halo radius if fit to the data). At lower beam energies, diffractive and stripping processes produce longitudinal momentum distributions that are similar in magnitude and width. At higher beam energies, stripping starts to dominate the one-neutron removal.

We have calculated also total cross sections as well as longitudinal momentum distribution for the breakup of ^{8}B. As the ground state of the proton is a p state, the discrepancy

between the transparent limit and full calculation is much more drastic in this case. The width of the full calculation is in good agreement with the experiments; the total cross sections are in fair agreement, with a discrepancy between the data of the two experiments.

At the moment our calculations are restricted to longitudinal momentum distributions. These are less sensible to the details of the interaction and more sensible to the structure of the halo and are therefore more easily interpreted. In the future we want to extend our calculations also to the transverse momentum distribution. In this case we have to include also the Coulomb potential in our calculation, especially in the case of ^{8}B. In the case of the diffraction we get a simple equation only for the relative momentum distribution between nucleon and core, which normally is not measured in experiments. But as measurements of the transverse momentum distribution have been done and more will be done in the future, it is interesting to see whether a single-particle model can describe their outcome.

ACKNOWLEDGMENTS

This work was supported in part by the Swiss National Science Foundation (SNF) and the ''Freiwillige Akademische Gesellschaft'' (FAG) of the University of Basel, and by the U.S. Department of Energy, Nuclear Physics Division, under Contracts DE-FG-06-90ER-40561 and W-31-109-ENG-38.

[1] H. Esbensen, Phys. Rev. C **53**, 2007 (1996).
[2] H. Esbensen, in *Proceedings of the International Workshop XXIV in Hirschegg*, Austria, 1996, edited by H. Feldmeier, J. Knoll, and W. Noerenberg (Gesellschaft für Schwerionenforschung mbH, Darmstadt, 1996), pp. 321–330.
[3] R. Serber, Phys. Rev. **72**, 1008 (1947).
[4] R. J. Glauber, Phys. Rev. **99**, 1515 (1955).
[5] A. G. Sitenko, *Theory of Nuclear Reactions* (World Scientific, Singapore, 1990), Chap. 4.
[6] C. A. Bertulani and K. W. McVoy, Phys. Rev. C **46**, 2638 (1992).
[7] P. Banerjee and R. Shyam, Phys. Lett. B **349**, 421 (1995).
[8] H. Sagawa and N. Takigawa, Phys. Rev. C **50**, 985 (1994).
[9] F. Barranco, E. Vigezzi, and R. A. Broglia, University of Milano Report No. NTGMI-95-2, 1995 (unpublished).
[10] J. Hüfner and M. C. Nemes, Phys. Rev. C **23**, 2538 (1981).
[11] P. G. Hansen, Phys. Rev. Lett. **77**, 1016 (1996).
[12] R. L. Varner, W. J. Thompson, T. L. McAbee, E. J. Ludwig, and T. B. Clegg. Phys. Rep. **201**, 57 (1991).
[13] H. de Vries, C. W. de Jager, and C. de Vries, At. Data Nucl. Data Tables **36**, 495 (1987).
[14] G. Bertsch, H. Esbensen, and A. Sustich, Phys. Rev. C **42**, 758 (1990).
[15] H. Esbensen and G. F. Bertsch, Phys. Rev. C **46**, 1552 (1992).
[16] G. F. Bertsch, B. A. Brown, and H. Sagawa, Phys. Rev. C **39**, 1154 (1989).
[17] G. Giacomelli, *Total Cross Section Measurements: Progress in Nuclear Physics* (Pergamon, New York, 1970), Vol. 12; S. K. Charagi and S. K. Gupta, Phys. Rev. C **41**, 1610 (1990).
[18] L. Ray, Phys. Rev. C **20**, 1857 (1979).
[19] K. Yabana, Y. Ogawa, and Y. Suzuki, Nucl. Phys. **A539**, 295 (1992).
[20] R. Anne *et al.*, Phys. Lett. B **304**, 55 (1993).
[21] R. Anne *et al.*, Nucl. Phys. **A575**, 125 (1994).
[22] M. Fukuda *et al.*, Phys. Lett. B **268**, 339 (1991).
[23] I. Tanihata, T. Kobayashi, O. Yamakawa, S. Shimoura, K. Ekuni, K. Sugimoto, N. Takahashi, T. Shimoda, and H. Sato, Phys. Lett. B **206**, 592 (1988).
[24] I. Tanihata,, H. Hamagaki, O. Hashimoto, Y. Shida, N. Yoshikawa, K. Sugimoto, O. Yamakawa, T. Kobayashi, N. Takahashi, Phys. Rev. Lett. **55**, 2676 (1985).
[25] T. Kobayashi, in *Proceedings of the 1st International Conference on Radioactive Nuclear Beams*, Berkeley (World Scientific, Singapore, 1990).
[26] J. H. Kelley, S. M. Austin, R. A. Kryger, D. J. Morrissey, N. A. Orr, B. M. Sherrill, M. Thoennessen, J. S. Winfield, J. A. Winger, and B. M. Young, Phys. Rev. Lett. **74**, 30 (1995).
[27] W. Schwab *et al.*, Z. Phys. A **350**, 285 (1995).
[28] T. Kobayashi (unpublished).
[29] B. A. Brown, A. Csoto, and R. Sherr, Nucl. Phys. **A597**, 66 (1996).